Engineering Membrane Distillation with Nanofabrication: Design, Performance and Mechanisms

Environmental Science: Water Research and Technology

Revised: 20 April, 2020

Rui Huang [1,2], Zhiquan Liu [3], Yun Chul Woo [4,5], Wenhai Luo [6,7], Stephen R. Gray[8], Ming Xie [1*]

[1] Department of Chemical Engineering, University of Bath, Bath, BA2 7AY, United Kingdom

[2] School of Environment, Harbin Institute of Technology, Harbin 150090, China

[3] Key Laboratory for Water Quality and Conservation of the Pearl River Delta, Ministry of Education; Institute of Environmental Research at Greater Bay, Guangzhou University, Guangzhou 510006, China

[4] Department of Land, Water, and Environment Research, Korea Institute of Civil Engineering and Building Technology (KICT), 283, Goyang-Daero, Ilsanseo-Gu, Goyang-Si, Gyeonggi-Do, 10223, Republic of Korea

[5] Department of Civil and Environment Engineering, University of Science and Technology (UST), 217, Gajeong-Ro, Yuseong-Gu, Daejeon, 34113, Republic of Korea

[6] Sustainable Energy Systems Engineering Group, School of Engineering, Macquarie University, Sydney, NSW, 2109, Australia

[7] Beijing Key Laboratory of Farmland Soil Pollution Prevention and Remediation, College of Resources and Environmental Sciences, China Agricultural University, Beijing 100193, China

[8]Institute for Sustainable Industries and Liveable Cities, Victoria University, Melbourne, 8001, Australia

[*]Corresponding author. E-mail: mx406@bath.ac.uk

ABSTRACT

Anti-fouling and durability are two important parameters that are closely associated with the development and deployment of membrane distillation (MD). In this study, we reported a nanoimprinted, omniphobic polytetrafluoroethylene (PTFE) membrane with hierarchical rough structure for MD process. A highly ordered, circular surface pattern was first imparted to PTFE membrane substrate via nanoimprint technique. An ultra-thin TiO_2 layer was deposited onto the nanoimprinted membrane to create spherical hierarchical rough structure via atomic layer deposition as well as initiator for chemical fluorination of the membrane. The resultant, nanofabricated membrane exhibited a water contact angle of 155° and contact angle above 100° against a range of low surface tension liquids. In addition, the nanofabricated membrane displayed a high and stable water flux around 34 $Lm^{-2}h^{-1}$ for more than 24 hours, and nearly complete salts rejection with the presence of surfactant. Most importantly, the water flux recovery rate of the resultant membrane was more than 91.3% after three fouling-cleaning cycles, demonstrating an excellent fouling reversibility. The new strategy proposed here that combines nanoimprint technique and super-hydrophobic modification sheds light into developing MD membrane with considerable durability and anti-fouling performance.

Water Impact Statement

Membrane distillation (MD) holds promise for sustainable brine management. To achieve this goal, we presented a facile and green approach for MD membrane design combing nanofabrication and chemical modification. The resultant MD membrane demonstrated anti-wetting and high fouling reversibility in treatment of brine waste containing surfactant and foulants.

Graphical Abstract

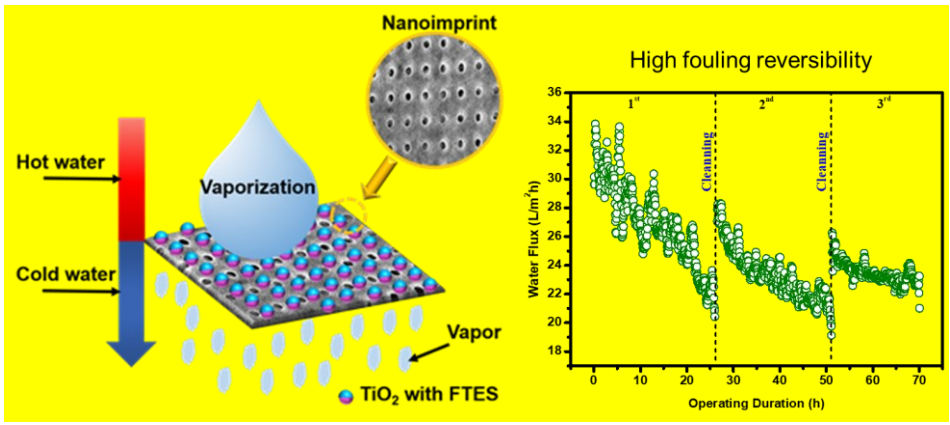
Nanoimprint
Hot water
Vaporization
Cold water
Vapor
TiO2 with FTES
High fouling reversibility
1st
2nd
3rd
Cleaning
Cleaning
Water Flux (L/m2h)
Operating Duration (h)

52

1. Introduction

Nowadays, water crisis has become an increasing concern all over the world due to severe water pollution and freshwater scarcity[1-3]. Although around 70% of the earth is covered by water, fresh water only accounts for 0.3%[4]. Therefore, it is imperative to develop reliable and economic technologies to treat seawater as an alternative source. Membrane distillation (MD), developed in recent decades, is a promising technology for seawater desalination and particularly for brine management and zero liquid discharge[5-7]. It is driven by the vapour pressure difference existing between the porous membrane surfaces, in which only vapour molecules are able to pass through the membrane[8]. Moreover, the heat energy that drive MD process could come from industrial waste heat[9]. Thus, MD is emerging as a viable technology for the desalination of seawater.

Membrane wetting is a primary barrier to widespread industrial use of MD, which is caused by partial or complete blocking of pores by liquid-phase water on the feed side[10, 11]. As a result, membranes for MD are usually fabricated using hydrophobic polymers, such as polyvinylidene fluoride (PVDF)[12], polypropylene (PP)[13], and polytetrafluoroethylene (PTFE)[14], to prevent wetting. Increasing membrane surface hydrophobicity could reduce capillary attraction of water into the membrane pore, thereby mitigating pore wetting[15]. Inspired by the feature of lotus leaf or sharkskin, super-hydrophobic membranes were first tailored by constructing a hierarchical rough structure combined with hydrophobic surface[16-18]. Hydrophobic surfaces with hierarchical rough structure can provide air pockets that decrease the total contact area between the membrane and water[19]. Grafting or mixing with low surface energy materials, such as fluoroalkyl-chains, on membrane surface is another common method to increase hydrophobicity[20].

Increasing surface hydrophobicity could however exacerbate membrane fouling. Because of strong hydrophobic-hydrophobic interactions, hydrophobic foulants can easily attach to the hydrophobic membrane surface and wick into the membrane pores, and thus adversely converts vapour transportation to direct liquid intrusion into the membrane pore[21]. To overcome this contradiction, researchers have developed Janus membranes with asymmetric wettability in more recent years[22, 23]. The outmost layer of Janus membranes is super-hydrophilic, which is designed to prevent mass transfer of foulants like micro oil drops. For example, Zhu et al.[24] developed a hydrophobic PVDF fibrous membrane substrate with a hydrophilic SiO_2/PAN skin layer,

demonstrating its stable performance in the treatment of high-salinity water containing a high concentration of lubricating oil. Nevertheless, these Janus membranes are much more difficult to tailor. Most of them suffer sacrificed breathability (water vapour transmission)[22, 25]. Thus, a simple method to construct both anti-wetting and anti-fouling MD membranes for the efficient desalination is required.

Nanoimprint, a simple and versatile nanofabrication technique, has been proposed for membrane fabrication[26, 27], which endows membrane surface with highly ordered features and thus can mitigate membrane fouling. Our previous study has proven that the PTFE membrane with periodical line pattern could significantly mitigate membrane fouling in MD process[28], due to significantly low adhesion force between foulants and patterned MD membrane surface. However, the durability of pristine PTFE nanoimprinted membranes was still unsatisfactory. Therefore, combining the nanoimprint technique with super-hydrophobic modification would have great potential to address wetting and fouling problems in MD process.

Herein, we presented a nanoimprinted, omniphobic membrane via nanoimprint technique, atomic layer deposition and fluorination, with the expectation to mitigate both membrane wetting and fouling. The fabricated membrane had a periodical circle pattern with hierarchical rough structure and low surface energy. The morphologies and chemical properties of the membrane were systematically characterized. Sodium dodecyl sulfate (SDS) and humic acid were chosen as the model contaminants to evaluate the durability and anti-fouling performance of the membrane. The green and facial method used here may be a potential candidate for brine management with complex compositions and varying foulants.

2. Materials and methods

2.1 Nanofabrication for membrane distillation

Nanofabrication was employed to engineer commercially available PTFE membrane (Durapore, 0.4 μm pore size, 280 μm thickness) with nanoimprint, atomic layer deposition of TiO_2 and fluorination by FTES (1H,1H,2H,2H-perfluorooctyltriethoxysilane) in tandem (Figure

1). The resultant membrane in the aforementioned procedure was denoted as C-PTFE, ALD and FTES, respectively.

ALD, as a thin film deposition technique, can control the thickness of thin films at the angstrom level based on sequential self-limiting, gas-solid surface reactions[29]. From deposition chemistry perspective, ALD proceeds via two half-reactions where reactants (precursors) are pulsed into reactor alternately and cycle-wise; while CVD is a continuous process where all reactants are supplied at the same time to grow the film. Another feature of ALD is that it is capable of low-temperature processing[30] compared to CVD deposition techniques, thereby being suitable for processing polymeric membranes.

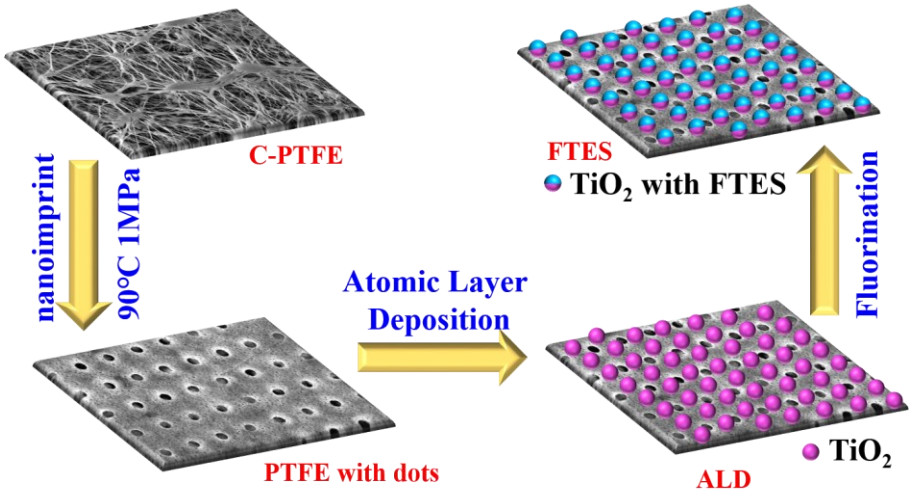

Figure 1: Schematic illustration of design and procedures for fabricating nanoimprint PTFE membrane with fluorinated TiO_2 deposition layer.

The PTFE membrane was first imparted with surface pattern by nanoimprinter (EVG 510, Thallner GmbH, Germany). Specifically, the PVDF membrane was placed on nickel substrate to ensure an even temperature. The silicon mask used possessed dot pattern with circle diameter of 6 μm and spacing (edge-to-edge) of 6 μm (Figure S1, Supplementary Data). The silicon mask was cleaned with acetone prior to the fabrication to clean off any debris from previous use. Patterning was carried out at 90 °C with a pressure of 1 MPa for 120 s, and the silicon mask was separated from the membrane samples at 35 °C. The pressure (i.e., piston force) and temperature were closely monitored during the nanoimprint to ensure sufficient surface patterns.

After nanoimprinting, we deposited an ultrathin layer of TiO_2 (around 5 nm in thickness) on the dot patterned MD membrane by atomic layer deposition (Fiji F200 ALD, Cambridge Nanotech). Tetrakis(dimethylamino) titanium (Strem Chemicals, Inc., USA), as known as TDMAT, and H_2O vapour were used as titanium and oxygen precursors, respectively. An ALD growth cycle of TiO_2 deposition consisted of the following steps and parameters: TDMAT pulse 0.1 s, N_2 purge 8 s, H_2O pulse 60 ms, N_2 purge 8s, deposition temperature at 120 °C. The total cycle of TiO_2 deposition was 125, resulting in TiO_2 thickness around 5 nm. The actual thickness of TiO_2 was estimated using a reference silicon wafer by a variable angle spectroscopic ellipsometer (J.A. Woollam M-2000DI).

Utilising the ultrathin film of TiO_2 on dot patterned MD membrane, we further functionalised it with FTES (1H, 1H, 2H, 2H-perfluorooctyltriethoxysilane). Specifically, hydroxylated FTES in toluene were prepared in 50 mL bottles through sonication and vigorous stirring for one hour, respectively. The coating procedure occurred in a glove box over 18 hours to obtain the resultant membrane, which was then washed with toluene and completely dried in an oven prior to use.

2.2 Membrane distillation apparatus and filtration protocol

Direct contact membrane distillation (DCMD) was conducted using a closed-loop bench-scale membrane test apparatus. The membrane cell was made of acrylic plastic to minimize heat loss to the surroundings. The flow channels were engraved in each of two acrylic blocks that made up the feed and permeate semi-cells. Each channel was 0.2 cm deep, 1.5 cm wide, and 1.5 cm long; and the total active membrane area was 2.25 cm^2. Temperatures of feed and distillate solutions were controlled by two heater/chillers (Polyscience, IL, USA), and were continuously recorded by temperature sensors that were inserted at the inlet and outlet of the membrane cell. Both feed and distillate streams were concurrently circulated by two gear pumps. The same crossflow rate of 30 L h^{-1} (corresponding to the crossflow velocity of 9 cm s^{-1}) was applied to both feed and distillate in order to minimize the pressure difference across the MD membrane. Weight change of the distillate tank was recorded by an electronic balance (Mettler Toledo, OH,

157 USA) with a data logger. All piping used in the DCMD test unit was covered with insulation
158 foam to minimize heat loss.

159 The nanofabricated MD membrane was subject to both wetting and fouling experiments.
160 Specifically, MD membrane wetting and fouling were simulated with feed solution containing 70
161 g L^{-1} NaCl solution (simulating seawater brine from reverse osmosis) with either 1 mM sodium
162 dodecyl sulfate (SDS) or 50 mg L^{-1} humic acid, respectively. In addition, MD membrane
163 fouling-cleaning cycle was conducted three times in order to examine the fouling reversibility
164 and cleaning efficiency by physical flushing. In the cleaning mode, the humic acid fouled MD
165 membrane was flushed by DI water at doubled cross flow rate (i.e., 18 cm s^{-1}) for 20 min. After
166 this brief, physical flushing, the fouling filtration resumed.

167 Feed and distillate volumes of four and one litre were used, respectively. Temperate of
168 inlet feed solution was 60 °C; while that of the distillate inlet stream was 20 °C in all
169 experiments. A new membrane sample was used for each experiment. Permeate mass was
170 recorded by a digital balance continuously. Conductivity of the distillate was measured by a
171 conductivity meter (HQ14d, Hach, CO) every 5 minutes.

172

173 **2.3 Characterization of nanofabricated membrane**

174 The nanofabricated MD membrane was comprehensively characterized in order to gain
175 insights in structure-performance relationship. Scanning electron microscopy (SEM), Fourier
176 transform infrared spectroscopy (FTIR), X-ray photoelectron spectroscopy (XPS), atomic force
177 microscopy (AFM) and thermo-gravimetric analysis (TGA) were employed to analyze the
178 morphology, thermal and physicochemical properties of the nanofabricated MD membrane.

179 Surface and cross-section morphology of the completely dried membranes with the gold
180 coating was visualized by EVO MA 10 (Zeiss, Germany) scanning electron microscope at an
181 accelerating voltage of 20 kV. AFM images were acquired with an Asylum Research MFP-3D
182 AFM operating in intermittent contact ("tapping") mode with a Budget Sensors TAP150Al-G
183 cantilever (f_R = 123 kHz, Q = 1745 and k = 2.1 Nm^{-1}, with free-air amplitude = 100 nm and
184 feedback set-point = 70 %).

To obtain information about composition and bonding chemistry of the MD membrane surface layer (with penetration depth from 1 to 5 nm thickness), X-ray photoelectron spectroscopy (XPS) analysis was carried out on monochromatic aluminium Kα X-ray photoelectron spectrometer (Thermo Scientific, MA). Survey spectra were recorded 3 times per sample, over the range of 0-1000 at 1 eV resolution to analyse the elemental composition. Bonding chemistry of membrane surface layer was analysed by high resolution C1s scan with XPS. A spot size of 400 μm was used to scan in the region of the C1s binding energy at 20 eV pass energy. Two random spots on duplicate membrane samples were selected. Excessive charging of samples was minimized using an electron flood gun. High resolution scans had a resolution of 0.1 eV. Calibration for the elemental binding energy was done based on the reference for carbon 1s at 284.6 eV. Data were processed by standard software with Shirley background and relative sensitivity factor of 0.278 for C1s peaks.

Membrane surface functional groups were identified using a Fourier Transform Infrared (FTIR) spectrometer (Thermo Scientific Nicolet 6700) equipped with an ATR accessory consisting of a ZnSe plate (45° angle of incidence). Absorbance spectra were measured with 64 scans of each sample at a spectral resolution of 2 cm^{-1}. Background measurements in air were collected before each membrane sample measurement. ATR-FTIR spectra were collected at two different spots for each membrane sample.

Membrane contact angle (CA) was measured by the sessile drop method using an optical subsystem (Theta Lite 100) integrated with an image-processing software. A range of liquids (water, diiodomethane, ethylene glycol and ethanol) were used for contact angle measurement.[31]

Thermal property of the nanofabricated MD membrane was quantified by thermo-gravimetric analysis (TGA) (Discovery TGA thermo-gravimetric analyser, SDT-Q600, United States) from 50 °C to 700 °C at a heating rate of 10 °C/min in N_2 atmosphere. The crucible material was platinum. Each sample was dried by purging N_2 for 1 min before measurement.

3. Results and Discussion

3.1 Characteristics of nanofabricated MD membrane.

3.1.1 Surface and structural characterization of the nanofabricated MD membrane

Commercially available hydrophobic PTFE membrane was chosen as scaffold for the subsequent nanofabrication procedure (Figure 1). PTFE membrane was firstly nanoimprinted and deposited with an ultrathin TiO_2 layer whose thickness was around 5.56 ± 0.11 nm, which was measured from the reference silicon wafer (Figure S2, Supplementary Data). Fiber-like texture of PTFE membrane surface disappeared, and membrane surface manifested a periodic, circular surface pattern. Compared with other coating techniques, atomic layer deposition can realize an extra-uniform TiO_2 layer. As a result, the membrane surface became smoother without obvious agglomerated TiO_2 nanoparticles.

A close examination of circular indentation shows elongated features in the vertical dimension, exhibiting hierarchy morphology. Besides, AFM image of TiO_2 deposition membrane (Figure 2E and F) shows the spherical hierarchical structure which might lead to a special wettability, thereby being beneficial to MD separation. After fluorination, there is no significant difference with ALD membrane, only scattered, tiny agglomerated particles could be observed. The FTES membrane still maintained a highly ordered dot pattern with smoother surface (Figure 2C).

Despite a series of modifications, the PTFE membrane was not compromised as evident in the cross-section of FTES membrane (Figure 2D), so that the resultant membrane could expect a satisfactory NaCl rejection in the MD filtration. Indeed, the membrane integrity of modified membrane remain uncompromised, which was evident by a 100% NaCl rejection in MD filtration. To re-cap, after modification, nanofabricated PTFE membrane exhibited a periodic, circular surface pattern with spherical hierarchical structure, while no noticeable compromise on membrane structure was observed.

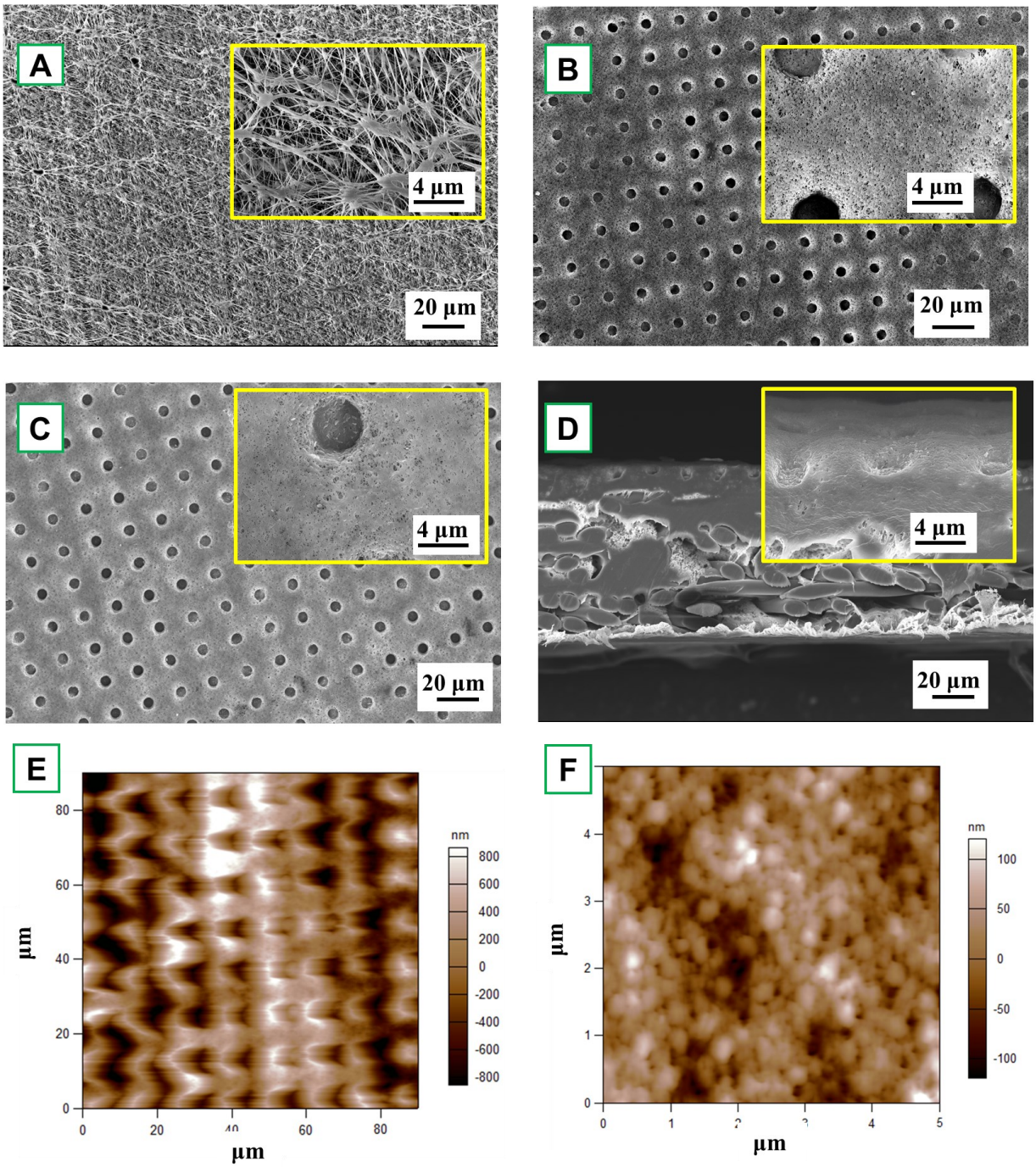

Figure 2: SEM images of membrane surface morphology: (A) pristine PTFE (C-PTFE); (B) TiO_2 atomic layer deposited nanoimprinted membrane (ALD); (C) fluorinated ALD membrane (FTES); (D) cross-section of FTES. Atomic Force Microscopy (AFM) imaging of (E) the membrane surface demonstrating the dot pattern and (F) deposition layer of TiO_2.

3.1.2 Chemistry characterization of the nanofabricated MD membrane

The surface modification of PTFE membrane with ALD and FTES was determined by ATR-FTIR and XPS, as shown in Figures 3A and 3B. Peak occurrence at wavenumbers of 839 and 875 cm^{-1} (red curve) suggests the bonding of TiO_2 nanoparticles onto membrane via ALD deposition. Reacting with anchoring TiO_2 nanoparticles, a fluorosilane surface modification was initiated involving hydrolysis and condensation of alkoxysilane groups with hydroxyl functional groups of the TiO_2 nanoparticles. The completion of this fluorosilane reaction was evident by the peak occurrence at wavenumbers of 1180 cm^{-1} and 1234 cm^{-1}, representing CF_2 and CF_3 bonds (blue curve). Indeed, the C1 scan of the resultant membrane showed the CF_2-CF_2 and CF_3 bonds on the membrane surface (Figure 3B). More importantly, the occurrence of CF_3 bond is the characteristic functional group possessing low surface energy that is favorable for MD performance, particularly in treatment of streams containing surfactants.

The composition of our modified membranes was further studied by thermo-gravimetric analysis (TGA). As shown in Figure 3C, the weight of C-PTFE, ALD and FTES kept stable when the temperature was below 350 °C. After that, the three membranes began to lose weight at 375.2 °C (ALD), 385.1 °C (FTES) and 391.1 °C (C-PTFE), respectively. There was a consistent shift of thermal decomposition towards lower temperature of modified membranes (both ALD- and FTES-modified membranes), which indicates enhancement in thermal stability. Higher residual mass was observed for ALD modified membrane in comparison with FTES modified membrane indicating the dispersion of TiO_2 nanoparticles in the composite membrane that resulted to improved thermal properties. Another feature presented in the TGA diagram was that TiO_2 deposition on the membrane may catalyse more C-PTFE loss.

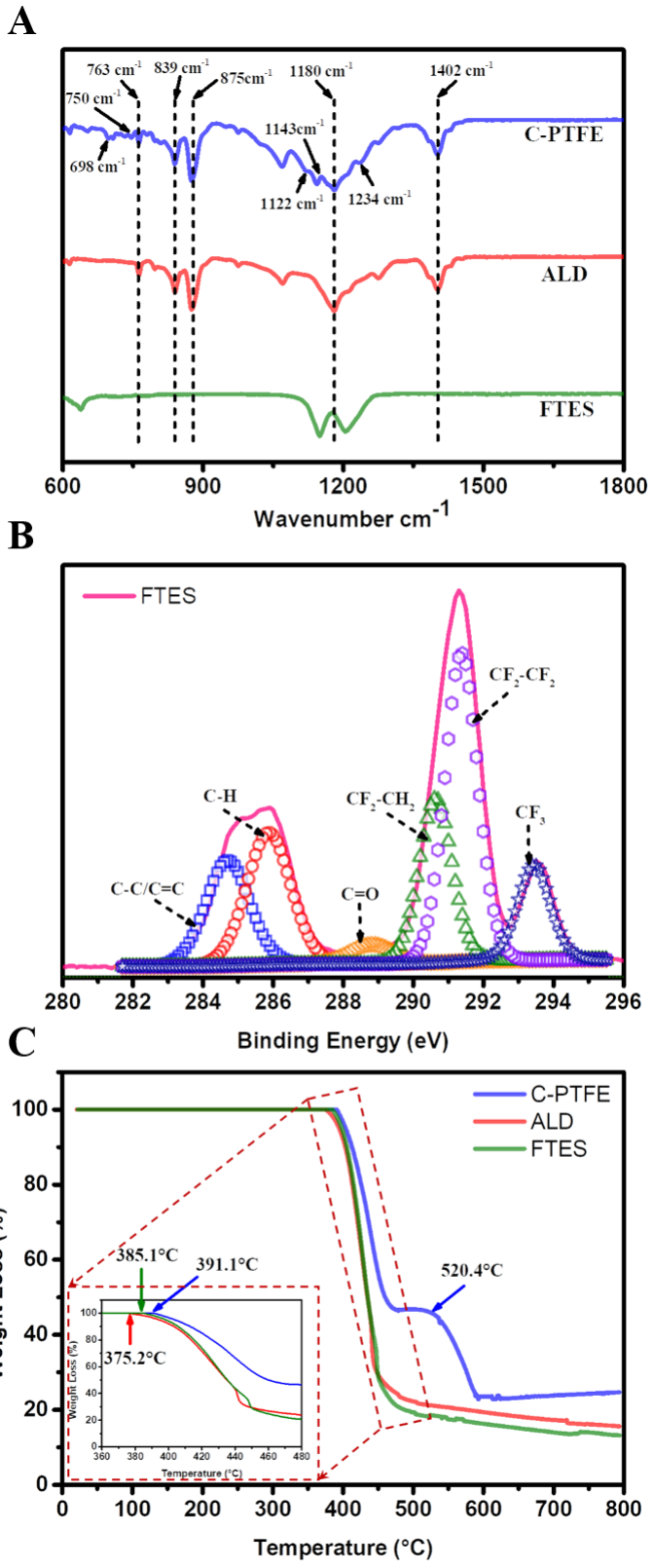
A
763 cm-1
839 cm-1
875cm-1
1180 cm-1
1402 cm-1
750 cm-1
1143cm-1
698 cm-1
1122 cm-1
1234 cm-1
C-PTFE
ALD
FTES
600
900
1200
1500
1800
Wavenumber cm-1
B
FTES
CF2-CF2
C-H
CF2-CH2
CF3
C-C/C=C
C=O
280
282
284
286
288
290
292
294
296
Binding Energy (eV)
C
C-PTFE
ALD
FTES
385.1°C
391.1°C
520.4°C
375.2°C
Weight Loss (%)
Temperature (°C)
0
20
40
60
80
100
0
100
200
300
400
500
600
700
800

263

Figure 3: Chemistry characterization of C-PTFE, ALD and FTES modified membranes. (A) ATR-FTIR spectra; (B) XPS spectra of C1s of FTES modified membrane; and (C) TGA curves.

3.2 Wetting properties of the nanofabricated MD membrane

The surface wettability of relevant nanofabricated membranes was measured using static water and low surface tension liquids (diiodomethane, ethylene glycol and ethanol) contact angles as shown in Figure 4. C-PTFE exhibited a high water contact angle of 135°, due to its hydrophobic nature. After the TiO_2 deposition, the contact angle decreased to 112°. TiO_2 can produce oxygen vacancies on its surface, which could be occupied by water molecules and produce adsorbed -OH groups. Thus, the membrane coated by TiO_2 tended to have a more hydrophilic surface, as demonstrated by lower WCA. By contrast, the fluorination by FTES endowed the ALD with extremely high water contact angle of 155°, thereby rendering a low surface energy as well as manifesting excellent hydrophobicity.

The ALD deposition created a hierarchically rough nanostructure. Based on the Wenzel and Cassie's theory, establishment of nano/microscale structures was essential for improving the super-hydrophobicity of a membrane. The contact angles of low surface tension liquids had the same tendency with water for similar reasons. As a result, the super-hydrophobic surface of FTES is expected to have a robust stability for MD applications.

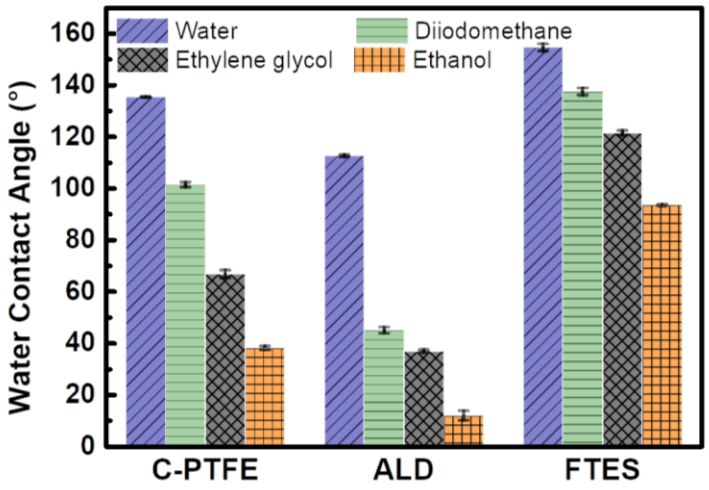

Figure 4: Water and low surface tension liquids (diiodomethane, ethylene glycol and ethanol) contact angles of C-PTFE, ALD and FTES modified membranes. Error bars indicate the standard deviation of three repeated measurements from two membrane samples.

3.3 Nanofabricated MD membrane exhibited anti-wetting behaviour

To further examine the role of fluorinated, hierarchically rough, nanostructure membrane surface, we compared the wetting behavior of ALD and FTES membranes to the pristine PTFE membrane using saline feed containing 1 mM SDS. The wetting phenomenon was quantified as the increase of permeate conductivity (Figure 5). It was observed that the permeate conductivity of pristine PTFE membrane soared sharply at the beginning, indicating the occurrence of membrane wetting. Although the pristine PTFE membrane is intrinsically hydrophobic, a declining trend in the rejection of NaCl over time was observed, which was consistent with membrane wetting during filtration. By contrast, after TiO_2 ALD modification, the permeate conductivity maintained stable for 20 hours. We attribute it to its hierarchically rough nanostructure. Despite the relatively low water contact angle, the hierarchically rough nanostructure could create air pockets on the membrane surface[19], and thus mitigate membrane wetting. In comparison, FTES modified membrane was able to sustain MD performance. The nanofabricated surface that achieved by fluorination and hierarchically rough nanostructure could successfully preserve a metastable Cassie-Baxter state (liquid-air interface) that prevents the membrane from being wetted[32-34].

Profiles of water flux during the filtration also confirmed the occurrence of membrane wetting (Figure 5B). The pristine PTFE was subject to a rapid flux decline. More importantly, surfactant in the feed can wick into the membrane pores with ease, preventing the transfer of vapor across the membrane. While the TiO_2 ALD and FTES modified MD membranes could maintain relatively steady water flux. In addition, it was noteworthy that the water flux of the FTES modified membrane (34 $Lm^{-2}h^{-1}$) was lower than TiO_2 ALD membrane (55 $Lm^{-2}h^{-1}$). This difference could be attributed to the fact that the increase in the thickness of the MD membrane slightly increased the resistance of water vapour transmission.

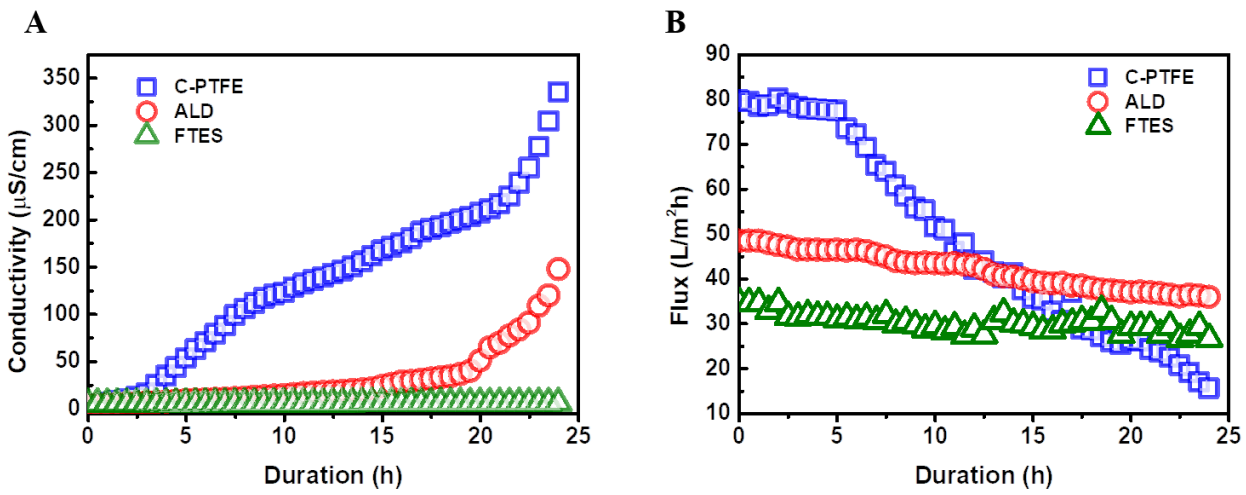

311

312 **Figure 5**: Comparison of filtration performance of C-PTFE, ALD and FTES modified
313 membranes: (A) permeate conductivity and (B) water flux.

314

315 **3.4 Nanofabricated MD membrane possessed high fouling reversibility**

316 One important hindrance in deploying MD membrane for challenging waste streams is
317 membrane fouling and fouling reversibility after cleaning. MD membrane possessing fluorinated
318 hierarchically rough nanostructure membrane surface was challenged in three fouling-cleaning
319 cycles where a brief (20 minutes), physical membrane flushing (doubling crossflow velocity)
320 using DI water was carried out as membrane cleaning. A highly satisfactory water flux recovery
321 was observed in the second and third cycles, achieving water flux recovery of 91.3% and 97.1%,
322 respectively (Figure 6b). Such high water flux recovery could be attributed to the nanostructured
323 surface pattern on the MD membrane. A highly ordered periodic, circular surface pattern can
324 potentially minimize the foulant-membrane interaction during the filtration. This high fouling
325 reversibility was consistent with our previous results and recent literature[35-38]. Apart from the
326 topological perspective, the fluorinated TiO_2 thin film layer on the membrane surface also
327 renders high slip property (low adhesion) against foulants during filtration. Indeed, the patterned
328 surface with floriation may alter the foulant deposition from pinned state to suspended state[38].
329 Similar observations were also reported in gypsum scaling in MD process by a superhydrophobic
330 micropillared PVDF membrane[39]. Both factors contributed to the excellent fouling reversibility,
331 which is vital for sustainability and robust MD membrane filtration for wastewater treatment.

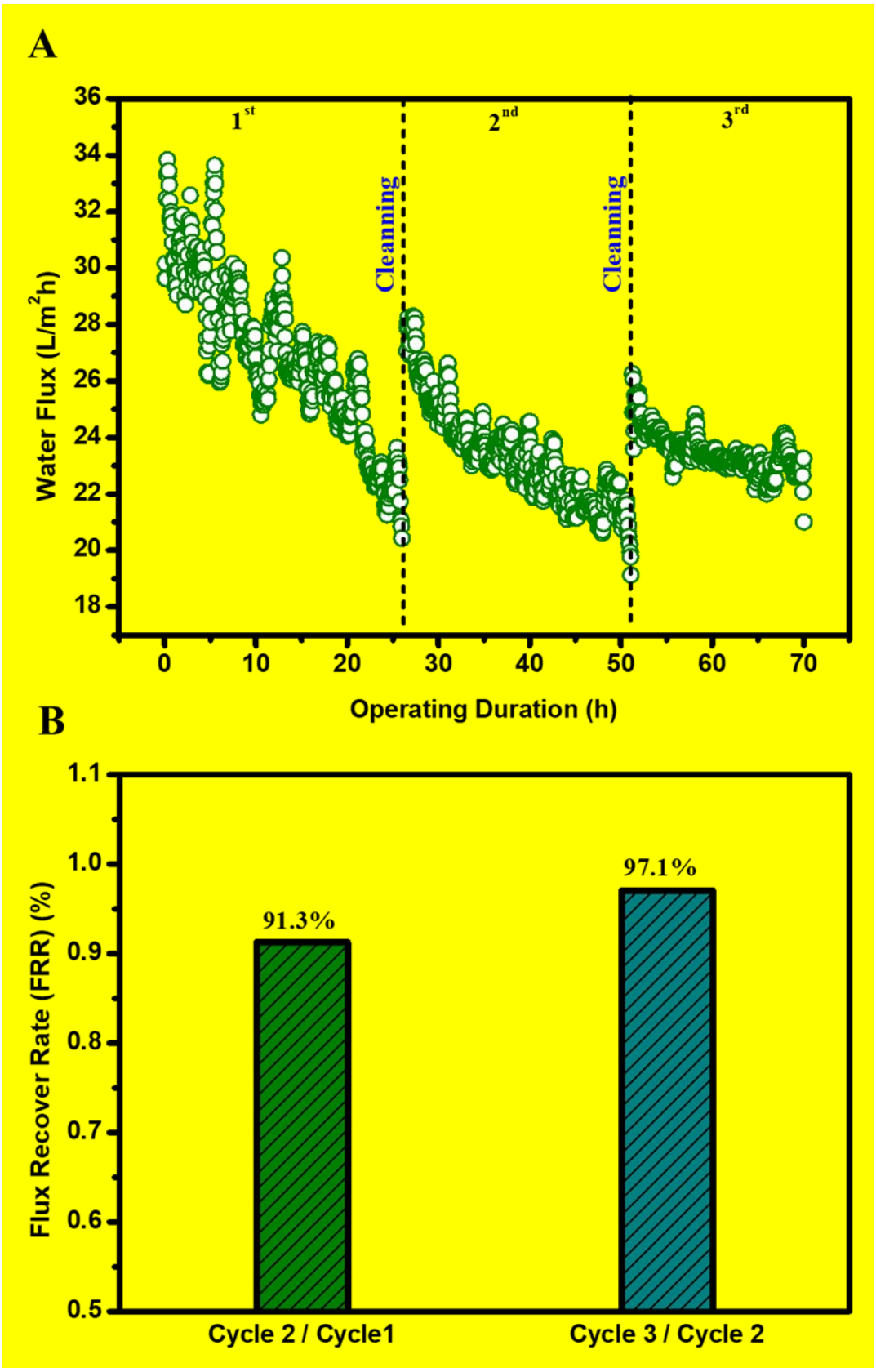
A
Water Flux (L/m²h)
Operating Duration (h)
1st
2nd
3rd
Cleanning
Cleanning
B
Flux Recover Rate (FRR) (%)
91.3%
97.1%
Cycle 2 / Cycle1
Cycle 3 / Cycle 2

332

Figure 6: Performance of FTES modified membrane in membrane distillation using three fouling-cleaning cycles (A) water flux decline curve; and (B) calculated water flux recovery rate after each cycle. The water flux recovery was calculated as the ratio between initial water fluxes of two consecutive filtration cycles.

4. Conclusion

Results reported here demonstrated a facile and scalable method to fabricate a nanopatterned, omniphobic PTFE membrane via nanoimprinting, atomic layer deposition (ALD), and fluorination for membrane distillation. The nanofabricated MD membrane was imparted with a highly ordered circle pattern and spherical hierarchical rough structure, thereby generating super-hydrophobicity with a water contact angle of 155° and anti-wetting potency for low surface tension liquids. As a result, the nanofabricated MD membrane manifested robust durability with a high and stable water flux around 34 $Lm^{-2}h^{-1}$ for more than 24 hours, and near 100% salt rejection in the presence of low surface tension surfactant. More importantly, our modification imparted fouling reversibility, achieving over 91.3% water flux recovery in three fouling-cleaning cycles.

5. Acknowledgements

This work was performed in part at the Melbourne Centre for Nanofabrication (MCN) in the Victorian Node of the Australian National Fabrication Facility (ANFF). R.H. thanked support from China Scholarship Council.

6. References

1. Y. Jiang, *Environmental Science & Policy*, 2015, **54**, 106-125.
2. M. Hanna-Attisha, J. LaChance, R. C. Sadler and A. Champney Schnepp, *American journal of public health*, 2016, **106**, 283-290.
3. F. Boltz, N. L. Poff, C. Folke, N. Kete, C. M. Brown, S. S. G. Freeman, J. H. Matthews, A. Martinez and J. Rockström, *Water Security*, 2019, **8**, 100048.
4. I. Aselmann and P. Crutzen, *Journal of Atmospheric chemistry*, 1989, **8**, 307-358.
5. S. K. Hubadillah, M. H. D. Othman, T. Matsuura, M. A. Rahman, J. Jaafar, A. Ismail and S. Z. M. Amin, *Sep. Purif. Technol.*, 2018, **205**, 22-31.
6. J. Chang, J. Zuo, K.-J. Lu and T.-S. Chung, *Desalination*, 2019, **449**, 16-25.

7. J. Guo, B. J. Deka, K.-J. Kim and A. K. An, *Desalination*, 2019, **468**, 114054.

8. A. Alkhudhiri, N. Darwish and N. Hilal, *Desalination*, 2012, **287**, 2-18.

9. R. D. Gustafson, S. R. Hiibel and A. E. Childress, *Desalination*, 2018, **448**, 49-59.

10. X. An, Z. Liu and Y. Hu, *Desalination*, 2018, **432**, 23-31.

11. M. Rezaei, D. M. Warsinger, M. C. Duke, T. Matsuura and W. M. Samhaber, *Water Res.*, 2018, **139**, 329-352.

12. K. Li, D. Hou, C. Fu, K. Wang and J. Wang, *Journal of Environmental Sciences*, 2019, **75**, 277-288.

13. Y. Shao, M. Han, Y. Wang, G. Li, W. Xiao, X. Li, X. Wu, X. Ruan, X. Yan and G. He, *Journal of membrane science*, 2019, **579**, 240-252.

14. W. Qin, J. Zhang, Z. Xie, D. Ng, Y. Ye, S. R. Gray and M. Xie, *Environmental Science: Water Research & Technology*, 2017, **3**, 119-127.

15. L. Dumée, V. Germain, K. Sears, J. Schütz, N. Finn, M. Duke, S. Cerneaux, D. Cornu and S. Gray, *Journal of membrane science*, 2011, **376**, 241-246.

16. M. Tang, D. Hou, C. Ding, K. Wang, D. Wang and J. Wang, *Sci. Total Environ.*, 2019, **696**, 133883.

17. H. Li, X. Zi, W. Shi, L. Qin, H. Zhang and X. Qin, *Membrane Water Treatment*, 2019, **10**, 287-298.

18. Y. Liao, G. Zheng, J. J. Huang, M. Tian and R. Wang, *Journal of Membrane Science*, 2020, **601**, 117962.

19. J. Ge, D. Zong, Q. Jin, J. Yu and B. Ding, *Adv. Funct. Mater.*, 2018, **28**, 1705051.

20. F. Guo, A. Servi, A. Liu, K. K. Gleason and G. C. Rutledge, *ACS applied materials & interfaces*, 2015, **7**, 8225-8232.

21. Y.-X. Huang, Z. Wang, J. Jin and S. Lin, *Environmental science & technology*, 2017, **51**, 13304-13310.

22. H.-C. Yang, W. Zhong, J. Hou, V. Chen and Z.-K. Xu, *Journal of Membrane Science*, 2017, **523**, 1-7.

23. Y. Liu, T. Xiao, C. Bao, Y. Fu and X. Yang, *Journal of membrane science*, 2018, **563**, 298-308.

24. Z. Zhu, Z. Liu, L. Zhong, C. Song, W. Shi, F. Cui and W. Wang, *Journal of Membrane Science*, 2018, **563**, 602-609.

25. J. H. Kim, S. H. Park, M. J. Lee, S. M. Lee, W. H. Lee, K. H. Lee, N. R. Kang, H. J. Jo, J. F. Kim and E. Drioli, *Energy & Environmental Science*, 2016, **9**, 878-884.

26. S. H. Maruf, L. Wang, A. R. Greenberg, J. Pellegrino and Y. Ding, *Journal of membrane science*, 2013, **428**, 598-607.

27. Z. Zhan and Y. Lei, *ACS nano*, 2014, **8**, 3862-3868.

28. M. Xie, W. Luo and S. R. Gray, *Water Res.*, 2017, **124**, 238-243.

29. S. M. George, *Chemical Reviews*, 2010, **110**, 111-131.

30. R. L. Puurunen, *Journal of Applied Physics*, 2005, **97**, 121301.

31. Y. Chul Woo, Y. Chen, L. D. Tijing, S. Phuntsho, T. He, J.-S. Choi, S.-H. Kim and H. Kyong Shon, *Journal of Membrane Science*, 2017, **529**, 234-242.

32. H. Y. Erbil and C. E. Cansoy, *Langmuir*, 2009, **25**, 14135-14145.

33. J. Lee, C. Boo, W.-H. Ryu, A. D. Taylor and M. Elimelech, *ACS applied materials & interfaces*, 2016, **8**, 11154-11161.

34. A. Sudeepthi, L. Yeo and A. Sen, *Appl. Phys. Lett.*, 2020, **116**, 093704.

35. Y.-J. Won, J. Lee, D.-C. Choi, H. R. Chae, I. Kim, C.-H. Lee and I.-C. Kim, *Environmental Science & Technology*, 2012, **46**, 11021-11027.

36. D.-C. Choi, S.-Y. Jung, Y.-J. Won, J. H. Jang, J.-W. Lee, H.-R. Chae, J. Lim, K. H. Ahn, S. Lee, J.-H. Kim, P.-K. Park and C.-H. Lee, *Environmental Science & Technology Letters*, 2017, **4**, 66-70.

37. J. A. Kharraz and A. K. An, *Journal of Membrane Science*, 2020, **595**, 117596.

38. Z. Xiao, H. Guo, H. He, Y. Liu, X. Li, Y. Zhang, H. Yin, A. V. Volkov and T. He, *Journal of Membrane Science*, 2020, **599**, 117819.

39. Z. Xiao, Z. Li, H. Guo, Y. Liu, Y. Wang, H. Yin, X. Li, J. Song, L. D. Nghiem and T. He, *Desalination*, 2019, **466**, 36-43.